Regular article

A matrine-oxymatrine in-situ gel for the treatment of allergic rhinitis

Peng Wu[a,b], Di Feng[a], Hongjian Wang[a], Shilin Li[a], Linghe Zang[c], Nan Liu[d], Yilin Wang[a], Dongchun Liu[a,b]*, Xing Tang[d]

[a] *School of Chinese Materia Medica, Shenyang Pharmaceutical University, Shenyang 110016, China;*
[b] *Joint International Research Laboratory of Intelligent Drug Delivery Systems of Ministry of Education, Shenyang Pharmaceutical University, Shenyang 110016, China;*
[c] *School of Clinical Pharmacy, Shenyang Pharmaceutical University, Shenyang 110016, China;*
[d] *School of Pharmacy, Shenyang Pharmaceutical University, Shenyang 110016, China*

Abstract

Sophorae Flavescentis **Radix (Ku Shen) is a traditional Chinese medicine used to treat damp-heat syndrome-related diseases, such as dysentery, jaundice, rhinitis, and skin inflammation. Recent studies have revealed the potential pharmacological value of its active alkaloid components, matrine (MAT) and oxymatrine (OMT), in the treatment of allergic rhinitis (AR). To develop a thermosensitive in-situ gel containing MAT and OMT for the intranasal treatment of AR, a thermosensitive matrix composed of Pluronic F127/F68 was optimized using the Box–Behnken Response Surface Methodology. The biosafety of the formulation was evaluated using a palatal ciliary movement model. A guinea pig model of AR induced by ovalbumin and aluminum hydroxide was established. Pharmacodynamic effects were comprehensively assessed through behavioral scoring, histopathological analysis (hematoxylin and eosin) of nasal mucosa, and serum immunological markers (IgE, IL-4, and IFN-γ). The MAT-OMT in-situ gel showed no toxicity during ciliary movement in the toad palatal ciliary motility model. The MAT-OMT combination significantly alleviated nasal itching, sneezing, and rhinorrhea in guinea pigs with AR, mitigated mucosal edema and epithelial damage, and improved inflammatory cytokine levels, suggesting its efficacy in correcting Th1/Th2 immune imbalance. The comprehensive therapeutic effect of MAT-OMT was significantly superior to that of MAT or OMT alone and comparable to that of the positive control, budesonide.**

Keywords: matrine; oxymatrine; combination; in-situ gel; allergic rhinitis

1 Introduction

Allergic rhinitis (AR), an IgE-mediated chronic inflammatory disorder of the nasal mucosa, is a critical public health challenge, with a global prevalence of over 40% in the past decade [1]. The pathogenesis of AR is mostly associated with the disruption of Th1/Th2 immune homeostasis, where Th2 cell hyperactivation drives the elevated secretion of cytokines (IL-4 and IL-5), subsequently promoting B-cell differentiation into IgE-producing plasma cells [2]. IgE binding to FcεRI receptors

* Author to whom correspondence should be addressed. Address: School of Chinese Materia Medica, Shenyang Pharmaceutical University, Shenyang 110016, China; Tel.: +86-24-23984318, +86-13889108973; E-mail: liudongchun@outlook.com, liudc@syphu.edu.cn.
These authors have no conflict of interest to declare.

Received: 2025-07-13 Accepted: 2025-10-23

on mast cells triggers degranulation and release of inflammatory mediators (histamine or leukotrienes). The clinical manifestation includes classical symptoms such as nasal pruritus, sneezing, and mucosal edema [3]. Current therapies, including intranasal corticosteroids, antihistamines, and leukotriene receptor antagonists have limitations such as local adverse effects (irritation and mucosal atrophy) and therapeutic resistance in refractory cases [4,5]. In China, researchers have been exploring the identification of effective therapeutic agents from traditional Chinese medicine (TCM) to address these limitations in the treatment of AR.

It is reported that nasal drops made from *Sophorae Flavescentis* Radix have demonstrated the good activities for the management of AR [6]. Matrine (MAT) and oxymatrine (OMT) are bioactive alkaloids isolated from the roots of *Sophora flavescens* Ait., which exhibit dual anti-inflammatory and anti-allergic activities by suppressing Th2 polarization and histamine release, highlighting their therapeutic potential [7,8]. MAT rapidly permeates cell membranes to suppress mast cell degranulation, but its performance is limited by rapid metabolism and relatively high toxicity [9-11]. In contrast, OMT exhibits improved water solubility, but its bioavailability is low, requiring metabolic conversion to the active form, MAT, for therapeutic effects [12,13]. This suggests that combined use of MAT and OMT may balance rapid onset and sustained efficacy. The MAT-OMT combination aligns with the clinical need for rapid relief of acute allergic rhinitis symptoms, including sneezing and nasal itching. However, conventional nasal drops are constrained by suboptimal mucosal retention (< 20 min) owing to mucociliary clearance [14,15]. Although viscosity enhancement prolongs residence time, high-viscosity gel formulations often fail to ensure accurate dosing and uniform drug distribution within the nasal cavity. To circumvent these challenges, in-situ gel systems have been developed for prolonged nasal drug delivery, with Pluronic F127 and Pluronic F68 being widely used as thermosensitive in-situ gel matrices [16-20]. Compared with single-component thermogelling systems, the dual-component thermosensitive in-situ gel system composed of Pluronic F127 and Pluronic F68 demonstrates enhanced tunability in phase transition behavior and mucoadhesive properties [21,22]. However, existing dual-component systems require further optimization to achieve ideal sustained-release kinetics and long-term nasal retention.

In this study, we developed a MAT-OMT co-loaded thermosensitive in-situ gel, hereafter referred to as the in-situ gel, for AR treatment. By incorporating glycerol as a third component into the Pluronic F127/F68 matrix, a novel ternary thermosensitive gel system was conducted via Box–Behnken Response Surface Methodology. We hypothesized that precise optimization of the ratios of Pluronic F127, F68, and glycerol would prolong the nasal residence time of the MAT-OMT drug combination by modulating the formulation's physicochemical properties, such as potential rheological behavior and mucosal interactions, thereby enhancing its overall therapeutic efficacy in a guinea pig ovalbumin-induced allergic rhinitis model. Safety was evaluated using a toad palatal ciliary motility model, and therapeutic efficacy was assessed in a guinea pig model of AR, with a preliminary investigation into the underlying mechanism.

2 Materials and methods

2.1 Ethical statement

Male toads (Bufo gargarizans; 100 ± 10 g) were procured from the Animal Experiment

Center of Shenyang Pharmaceutical University. Guinea pigs (Crl: HA Hartley; equal distribution by gender; 260–300 g) were obtained from Tianjin Yuda Experimental Animal Breeding Co., Ltd. (Tianjin, China; license no. SCXK(Jin)2021-0001). Upon arrival, all animals underwent a 7-day acclimatization period in climate-controlled housing (22 ± 1 °C, 55 ± 5% humidity, 12-h light/dark cycle) with ad libitum access to standard feed and water. Daily health monitoring revealed no abnormalities.

For guinea pig anesthesia, induction was achieved using a 4% isoflurane-oxygen mixture (flow rate: 1–2 L/min) followed by maintenance with 1-3% isoflurane during 30-min experimental procedures. Anesthetic depth was verified by loss of pedal withdrawal reflex and stable respiratory patterns (20–40 breaths/min). Post-experiment euthanasia was performed via cervical dislocation by certified personnel, in accordance with the AVMA Guidelines for the Humane Slaughter of Animals (2024 edition).

All animal experiments were approved by the Animal Experiment Ethics Committee of Shenyang Pharmaceutical University (NO. SYPU-IACUC-2024-0312-097), and were conducted in strict accordance with the university's regulations on laboratory animal management, the 3R principles, and the ARRIVE guidelines [23].

2.2 Materials

MAT and OMT standards, with a minimum purity of 98%, were sourced from Shanghai Aladdin Biochemical Technology Co., Ltd. (batch numbers M109803 and A111286, respectively). MAT and OMT were procured from Changzhou Kangli Pharmaceutical Co. Ltd. (Jiangsu, China). Pluronic F127 and Pluronic F68 were obtained from Wuhan Weisijie Biological Technology Co., Ltd., and glycerol was purchased from Yousuo Chemical Technology Co., Ltd., (Shandong, China). Vitamin E, with a purity > 95%, was sourced from Titan Scientific Technology Co., Ltd. (Chengdu, China). Analytical-grade methanol was obtained from Tianjin Kangkedai Chemical Reagent Factory (Tianjin, China), and chromatography-grade methanol was acquired from Beijing Decema Co., Ltd (Beijing, China).

2.3 Preparation of an in-situ gel

The in-situ gel was prepared using the cold solvent method [1-3] and optimized using a Box–Behnken Response Surface Methodology. Pluronic F127, Pluronic F68, glycerol, and vitamin E were completely dissolved in purified water. MAT and OMT were accurately weighed and incorporated into the gel matrix to yield a final concentrations of 1.0% *w/w* for each agent. The drug-excipient mixture was homogenized and refrigerated at 4 °C for 24 h to ensure the complete hydration of the polymer. A transparent, homogeneous, flocculation-free MAT-OMT in-situ gel formulation was obtained using this protocol.

2.4 Gel optimization

To optimize the in-situ gel formulation, a Box–Behnken Response Surface Methodology was applied using JMP software (version 14.0) to systematically adjust the concentrations of Pluronic F127 (A), Pluronic F68 (B), and glycerol (C). A statistical model was employed to characterize the effects of these formulation factors on the target gelation temperature, followed by an evaluation of the ANOVA table to assess the significance and predictive efficiency of the model. The experimental factor levels for the Box–Behnken design are presented in Table 1.

Table 1 Box–Behnken test factor levels

Levels	Factors		
	A Pluronic F127/%	B Pluronic F68/%	C glycerol/%
-1	15	1	2
0	20	3	7
1	25	5	12

2.5 Measurement of gelation temperature, gelation time, pH, and viscosity

The gelation temperature was determined by transferring 5 mL of the gel into a test tube immersed in a thermostatic water bath, with the gel surface maintained 2 cm below the water level. After 5 min of thermal equilibration (confirmed by temperature stabilization), a digital thermometer (JM222, 0.1 °C resolution) was positioned at the gel-air interface [26]. The temperature was incrementally raised at 0.1 °C/5-min interval until gelation onset—defined as zero flow upon a 30-s tube inversion—with triplicate measurements recorded [27].

The gelation time was assessed by equilibrating the MAT-OMT in-situ gel in tubes at ambient temperature (25 °C) for 10 min, followed by 60° tube tilting in a water bath. The sol-gel transition duration was measured using a digital stopwatch [28], and triplicate measurements were performed.

For pH determination, 1.0 mL of the gel was precisely diluted to 100 mL with distilled water using volumetric glassware. The pH of the resulting solution was measured in triplicate using a calibrated pH meter [26].

Viscosity analysis was achieved using an NDJ-8S rotational viscometer under controlled temperatures (25 °C and gelation temperature). Steady-state viscosity measurements were conducted using appropriate spindle speed combinations in triplicate [29].

2.6 Evaluation of homogeneity

Comparable quantities of the in-situ gel were procured from samples stored under ambient conditions and at the gelation temperature for 2 weeks. Each sample was subjected to centrifugation at 5000 r/min for 20 min. The purpose of this step was to examine whether phase separation occurred [30].

2.7 In vitro drug release studies

MAT and OMT were evaluated using a Waters 2695/2487 HPLC system with a COSMOSIL C_{18} column (5 μm, 4.6 mm × 250 mm). The mobile phase was methanol, 0.01% triethylamine solution = 75:25 (*v/v*) with a detection wavelength of 215 nm, a column temperature of 30 °C, a flow rate of 1.0 mL/min, and an injection volume of 10 μL.

Drug release studies were performed using an adapted Franz diffusion cell setup. The experiments were conducted with a receptor compartment volume of 6.5 mL and an effective diffusion area of 2.54 cm². The cells were maintained at a constant temperature in a circulating water bath. Precisely, 0.30 g of the formulated sample was weighed in triplicate and placed on a polytetrafluoroethylene filter membrane (0.45 μm) in the donor compartment. In the receptor compartment, 6.5 mL of artificial nasal fluid (ANF) was added. The ANF was prepared as a 13.6 g/L solution of potassium phosphate monobasic (KH_2PO_4), with the pH adjusted to 6.4 ± 0.1. Stirring

was initiated at 300 r/min with the temperature regulated at 33.5 ± 0.5 °C. Sampling was performed at 0.5, 1, 2, 4, 6, 8, 12, and 24 h, with 5 mL aliquots taken and replaced with an equal volume of freshly equilibrated receptor medium. The collected samples were filtered through 0.45 μm filters [31]. Cumulative release amounts Q_t ($\mu g \cdot cm^{-2}$) were calculated using the following formula:

$$Q_t = \sum_{i=1}^{n-1} C_n \times V + (C_i \times V_i)/A$$

Where Q_t ($\mu g \cdot cm^{-2}$) values are plotted against time t (h), and the slope of the linear portion of the curve represents the steady-state release rate, denoted as Jss ($\mu g \cdot cm^{-2} \cdot h^{-1}$). The intercept of the extrapolated straight-line segment with respect to the time axis yields the lag time t_{lag} (h).

Employing classical drug release models, with the sampling time denoted as t and the cumulative release fraction represented by Y, fitting was conducted using Origin 2018 software. The most appropriate model was chosen based on the experimental results and R_2 values. The correlation coefficient, R_2, closer to 1, indicates a better fit, reflecting an improved correspondence between the drug release profile and the corresponding equation.

2.8 Cilia toxicity studies

The palatal ciliary toxicity of the MAT-OMT in-situ gel was evaluated using the toad palatal ciliary motility model, a gold-standard method [32]. After piching to destroy the brains and spinal cords, the dissected palatal mucosa of each toad was fully immensed for 30 min in normal saline (0.5 mL) (control group), MAT-OMT in-situ gel (treatment group), blank in-situ gel (vehicle control group), or 1% sodium deoxycholate (positive control group). The mucosal specimens were rinsed with normal saline and meticulously dissected using ophthalmic scissors and forceps to isolate the buccal mucosa. After removing the blood clots and debris, the mucosa was positioned upward on the cilia side on glass slides for microscopic observation at 400× magnification. After observation, the specimens were transferred to chromatography columns filled with distilled water, sealed, and maintained at near-saturated humidity. Ciliary oscillation patterns were monitored microscopically at 10-min intervals until complete cessation. Post-cessation, mucosal specimens were phosphate-buffered saline-washed and re-evaluated. Persistent oscillation recovery prompted recording of total sustained palatal ciliary motility duration [33].

2.9 Establishment of an allergic rhinitis guinea pig model and drug administration protocol

After a 5-day acclimatization period, the guinea pigs were randomly allocated into six groups, each consisting of six animals. The AR model was established through systemic sensitization, followed by local stimulation (Fig. 1), mimicking natural disease progression. Local stimulation was achieved through nasal instillation. All animals except those in the normal control group received daily intraperitoneal injection of an allergen suspension (0.5 g ovalbumin as the antigen, 30 mg aluminum hydroxide powder as the adjuvant, and 1 mL saline) for 7 d (systemic sensitization). Subsequently, 5% ovalbumin was instilled into each nostril (50 μL per side) once daily for 5 consecutive d, eliciting a reaction (local sensitization). The control group received the same volume of saline solution. The AR induction protocol closely simulated the natural disease process, ensuring the relevance and validity of the model. Drug administration began the day after the antigen challenge. The therapeutic solutions were instilled into the nostrils of the guinea pigs (50 μL per side) three times daily for 11 consecutive d. Nasal administration was performed on conscious animals to avoid suppression of natural allergic

responses such as sneezing and nasal itching, which are critical for pharmacodynamic evaluation [34].

The control and model groups received an equivalent volume of placebo. Throughout this period, 5% ovalbumin was concurrently instilled into the nasal cavity (50 μL per side) three times daily, 1 h prior to drug administration, to stimulate the nasal passages of the animals. This protocol ensured that the treatment groups were exposed to the allergen challenge while receiving the respective medications, enabling the evaluation of their therapeutic effects on the established AR model [1].

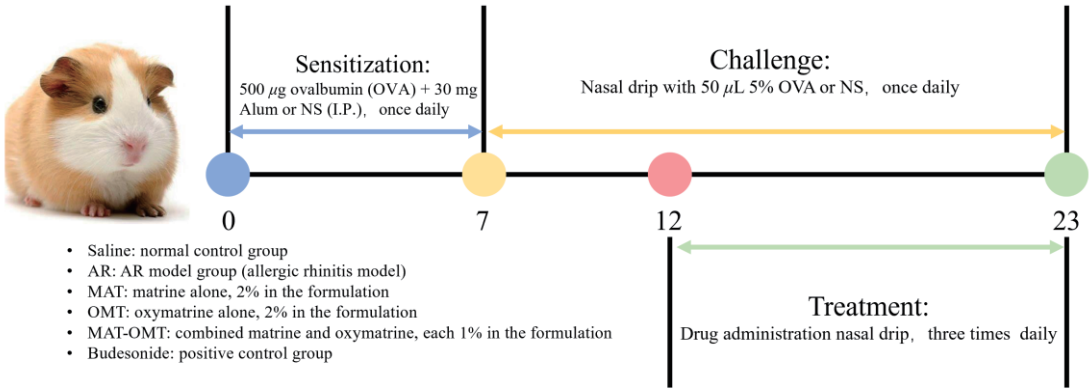

Fig. 1 Schematic diagram of treatment in the ovalbumin-induced AR murine model

2.10 Observation of rhinitis symptoms and behavioral scoring

Within 30 min after the final stimulation, the guinea pigs were placed in transparent observation chambers for individual assessment and scored for the severity of nasal itching, sneezing, and clear mucus discharge [34]. The total score was calculated cumulatively for each symptom. A total symptom score above five points indicated successful model development [35]. Behavioral scores were recorded after the final administration in both the modeling and treatment phases to evaluate modeling efficacy and treatment response. Symptoms before treatment were assessed immediately after the final nasal challenge during modeling, and those after treatment were assessed after the final nasal challenge during treatment. To minimize bias, symptom scoring was conducted by researchers unaware of the experimental group allocation of each guinea pig.

Symptom scoring was performed according to established criteria [8] as follows: Nasal itch: mild, 1 point (gentle nose rubbing several times); moderate, 2 points (frequent nose rubbing); severe, 3 points (persistent scratching of the nose and face, rubbing against surfaces). Sneezing: 1–3 sneezes, 1 point; 4–10 sneezes, 2 points; 11 or more sneezes, 3 points. Rhinorrhea: reaching the nostril openings, 1 point; extending beyond the nostrils, 2 points; mucus flowing over the face, 3 points.

2.11 Hematoxylin and Eosin (H&E) tissue staining

After blood collection, the guinea pigs were euthanized and the nasal skin was rapidly excised [36]. The maxilla, along with the nasal cavity, was collected from the mid-incisor region. The bilateral nasal turbinates and septal mucosa were meticulously removed and fixed in 4% paraformaldehyde [37]. Subsequently, the tissues underwent standard histological processing, including dehydration, clearing, wax impregnation, and embedding in paraffin blocks. Four-micron-thick sections were prepared using a rotary microtome and

stained with H&E. The slides were then examined under an optical microscope to compare the degree of inflammatory infiltration in the nasal mucosas of the sensitized guinea pigs.

2.12 Inflammatory cytokine levels

The concentrations of IgE, IL-4, and TNF-γ in the serum samples were quantified using ELISA [38]. according to the the manufacturer's protocol. Absorbance was measured at 450 nm using a microplate reader. The average results were reported after each measurement was performed thrice.

2.13 Statistical analysis

All data are represented as means ± SD from six animals per group. The normality of data distribution was confirmed using the Shapiro-Wilk test prior to parametric analysis ($P > 0.05$ for all datasets). Group differences were compared using one-way ANOVA and *t*-tests with the SPSS 11.5 software. Statistical significance was set at $P < 0.05$, with $P < 0.01$ considered highly significant.

3 Results

3.1 Box–Behnken design and response surface methodology

Table 2 shows the Box–Behnken experimental factor levels. To determine gelation temperature (33.5 °C) based on Pluronic F127 (range: 15–25%), Pluronic F68 (range: 1–5%), and glycerol (range: 2–12%), 15 experimental runs (formulas) were suggested by the JMP software (version 14.0). In addition, the associated ANOVA table was used to analyze the quadratic model (Table 3).

Table 2 Box–Behnken experimental design and results

Formula/Run No.	A	B	C	Gelation temperature/°C
1	15	1	7	32.1 ± 0.5
2	15	3	2	46.2 ± 0.1
3	15	3	12	38.7 ± 0.2
4	15	5	7	43.2 ± 0.1
5	20	1	2	22.6 ± 0.1
6	20	1	12	18.6 ± 0.1
7	20	3	7	23.5 ± 0.4
8	20	3	7	22.2 ± 0.8
9	20	3	7	22.8 ± 0.1
10	20	5	2	32.2 ± 0.3
11	20	5	12	22.9 ± 0.1
12	25	1	7	13.6 ± 0.2
13	25	3	2	18.0 ± 0.4
14	25	3	12	12.6 ± 0.1
15	25	5	7	16.3 ± 0.5

Note: The data are presented as means ± SD from three independent experiments.

Table 3 ANOVA results of the regression model

Source	Sum of squares	df	Mean square	*F*-value	*P*-value	
Model	1526.97	9	169.66	78.77	< 0.0001	significant
A	1242.51	1	1242.51	576.88	< 0.0001	
B	95.91	1	95.91	44.53	0.0011	
C	85.81	1	85.81	39.84	0.0015	
AB	17.64	1	17.64	8.19	0.0353	
AC	1.10	1	1.10	0.5119	0.5063	
BC	7.02	1	7.02	3.26	0.1308	
A^2	63.08	1	63.08	29.29	0.0029	
B^2	1.64	1	1.64	0.7619	0.4227	
C^2	13.45	1	13.45	6.24	0.0546	
Residual	10.77	5	2.15			
Lack of Fit	9.92	3	3.31	7.81	0.1156	not significant
Pure Error	0.8467	2	0.4233			
Cor Total	1537.74	14				

In this model, factors A, B, and C correspond to Pluronic F127, Pluronic F68, and glycerol, respectively. The results of the regression model variance analysis are presented in Table 3; the Model *F*-value of 78.77 implies the model is significant ($P < 0.01$). In this case, A, B, C, AB, and A^2 are significant model terms ($P < 0.05$). The Lack of Fit *F*-value of 7.81 implies that it is not significant relative to the pure error ($P = 0.1156$).

Based on the experimental results, the following quadratic multiple regression equation was obtained:

$$Y = 22.83 - 12.46A + 3.46B - 3.28C - 2.1AB + 0.525AC + 4.13A^2 - 0.667B^2 + 1.91C^2$$

Analysis of the *F*-values revealed that Pluronic F127, Pluronic F68, and glycerol exerted significant influences on the gelation temperature, with their impact ranking as Pluronic F127 > Pluronic F68 > glycerol.

The contour and surface plots in Fig. 2 revealed significant differences in interaction strength. The surface plot of Pluronic F127 and Pluronic F68 exhibited the steepest slope, demonstrating a greater interaction between AB than that between BC (Pluronic F68 and glycerol), and AC (Pluronic F127 and glycerol). Overall, the interaction strengths ranked as AB > AC > BC.

The physiological temperature of the nasal cavity ranges from 32 to 35 °C, with a median value of 33.5 °C. Accordingly, 33.5 °C was set as the target gelation temperature. The optimized formulation derived under these parameters comprised 17.0% Pluronic F127, 3.0% Pluronic F68, and 5.0% glycerol (Table 4). Triplicate validation experiments yielded a mean gelation temperature of 33.2 °C, demonstrating close alignment with the predicted value (33.5 °C). These results confirm the robust predictive accuracy of the model.

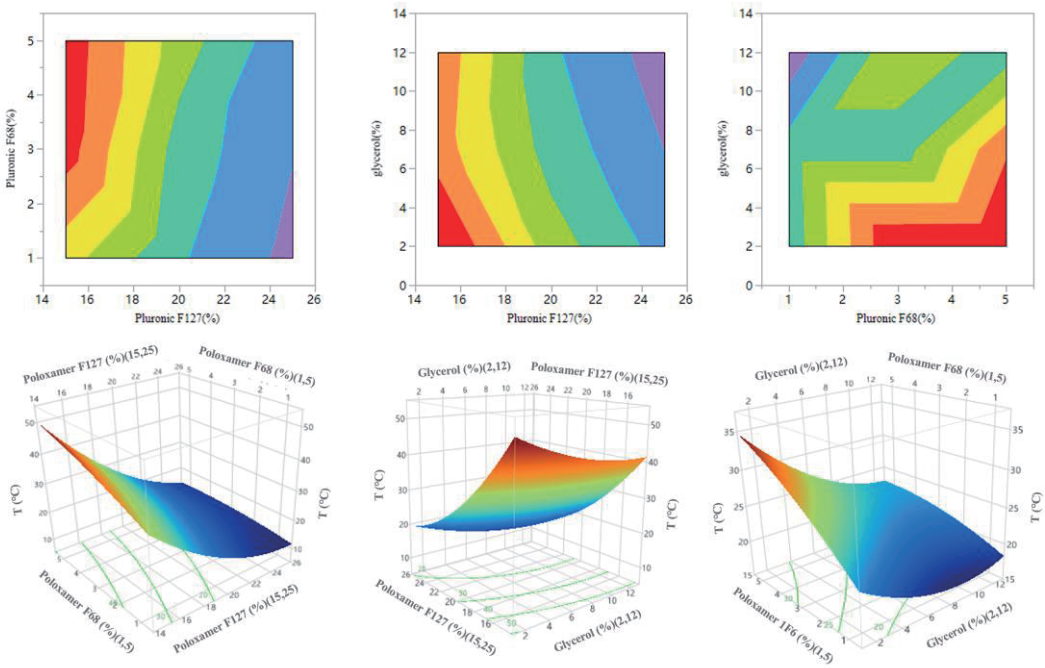

Fig. 2 Contour and surface plots of MAT-OMT in-situ gels

Table 4 Composition of the optimized MAT-OMT in-situ gel

Inputs	%(*W/W*)
Matrine	1.00
Oxymatrine	1.00
Pluronic F127	17.00
Pluronic F68	3.00
Glycerol	5.00
Vitamin E	0.02
H_2O	72.98
Total	100.00

3.2 Characterization

As shown in Fig. 3, the optimized in-situ gel demonstrated temperature-sensitive characteristics. After 2 weeks of storage at ambient temperature (25 °C) and the gelation temperature (33.5 °C), centrifugation at 5000 rpm for 20 min revealed no phase separation, with the gel maintaining its transparency and homogeneity. The formulated gel exhibited a gelation temperature of 33.5 ± 0.5 °C, aligning precisely with the physiological nasal temperature range (32–35 °C). Gelation occurred within 10.3 ± 0.5 s, with a physiologically compatible pH of 6 for nasal administration. Rheological characterization demonstrated temperature-responsive viscosity modulation: 7098 ± 210 mPa·s at 25 °C versus 159,833 ± 4,850 mPa·s at 33.5 ± 0.5 °C, ensuring prolonged nasal retention post-phase transition.

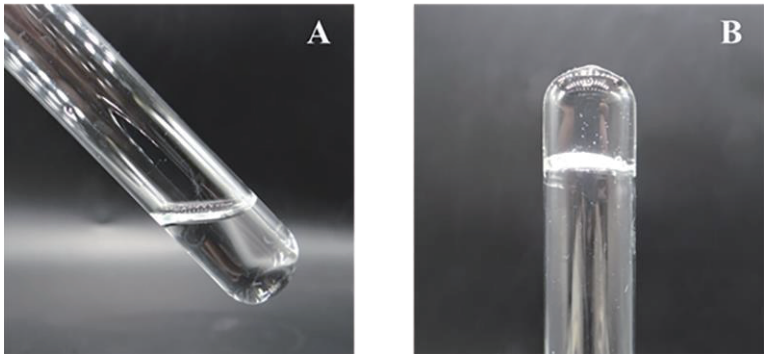

Fig. 3 Optimized in-situ gel at 25 °C (A) and at 33.5 °C (B)

3.3 In vitro drug release studies

We conducted a release study of the optimized MAT-OMT in-situ gel (Fig. 4 and Table 5). Over 24 h, the cumulative release amount (Q_{24}) of MAT was 934.17 $\mu g \cdot cm^{-2}$, corresponding to a cumulative release rate of 77.16%. For OMT, the Q_{24} was 831.17 $\mu g \cdot cm^{-2}$, with a cumulative release rate of 68.66%. After 12 h, the release profile plateaued. Compared with the various release models, both MAT and OMT exhibited favorable fit to the Ritger–Peppas Release and Weibull equation (Table 6).

The cumulative release rates of the MAT-OMT in-situ gel were less than 30% within the first 0.5 to 2 h, indicating the absence of a burst effect. Moreover, the sustained drug release lasted for over 12 h, demonstrating the potential of a controlled-release system.

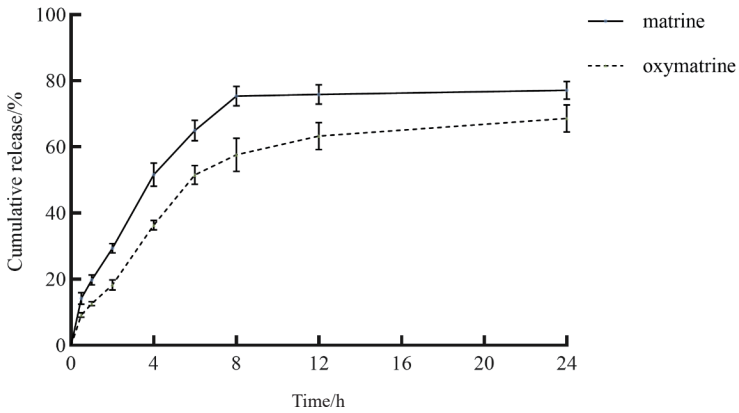

The data are presented as means ± SD from three independent experiments.

Fig. 4 *In vitro* cumulative drug release of the optimized MAT-OMT in-situ gel

Table 5 Release parameters of the optimized MAT-OMT in-situ gel

Parameter	Matrine	Oxymatrine
Q_{24} /($\mu g \cdot cm^{-2}$)	934.17 ± 38.04	831.17 ± 53.65
Q_t-t	$Q_t = 3.23 \cdot t + 47.48$	$Q_t = 3.77 \cdot t + 30.02$
J_{SS}/($\mu g \cdot cm^{-2} \cdot h^{-1}$)	3.23	3.77
T_{lag} /h	-14.69	-7.96
Release/%	77.16	68.66

Table 6 Drug release model fitting for the optimized MAT-OMT in-situ gel

Drug	Release model	Fitting equation	R^2
Matrine	Zero-order Kinetic Equation	$Y = 0.0261t + 0.3218$	0.5214
	First-order Kinetic Equation	$\ln(1-Y) = -0.0587t - 0.4265$	0.6062
	Higuchi Kinetic Equation	$Y = 0.1714\ t^{½} + 0.1079$	0.7686
	Weibull Kinetic Equation	$\ln(1/(1-Y)) = 0.4161\ln t + 0.2804$	0.9725
	Ritger–Peppas Release Kinetic Equation	$\ln Y = 0.5086\ln t - 1.5401$	0.9138
Oxymatrine	Zero-order Kinetic Equation	$Y = 0.0256t + 0.2135$	0.6509
	First-order Kinetic Equation	$\ln(1-Y) = -0.04716t - 0.2401$	0.7560
	Higuchi Kinetic Equation	$Y = 0.1612\ t^{½} + 0.0190$	0.8601
	Weibull Kinetic Equation	$\ln(1/(1-Y)) = 0.3087\ln t + 0.1577$	0.9879
	Ritger–Peppas Release Kinetic Equation	$\ln Y = 0.5920\ln t - 1.9588$	0.9392

3.4 Examination of cilia toxicity

We evaluated the potential cytotoxicity of the optimized MAT-OMT in-situ gel on normal cilia using a toad cilia model (Table 7). The cilia oscillation duration for the normal control group was 843.33 ± 13.23 min. The cilia persistence time following administration of the MAT-OMT in-situ gel was 831.33 ± 6.21, compared with 835.67 ± 3.01 min for the blank gel matrix. These values were not significantly different from those of the control group ($P > 0.05$), with relative percentages of 98.58% and 99.09%, respectively. In contrast, the sodium deoxycholate group had a cilia oscillation duration of 45.33 ± 2.88 min, which was significantly different from the normal control group ($^{**}P < 0.01$). According to literature, a higher percentage indicates less impact on palatal ciliary movement, suggesting lower ciliotoxicity [39]. These findings suggest that both the MAT-OMT in-situ gel and blank gel matrix have negligible ciliotoxicity, indicating a certain level of safety for nasal administration.

Table 7 Effect of the optimized MAT-OMT in-situ gel on oscillation time of cilia in the mucosa of a toad palate

Parameter	Saline group	MAT-OMT in-situ gel group	Blank in-situ gels group	Sodium deoxycholate group
Cilia persistence times /min	843.33 ± 13.23	831.33 ± 6.21	835.67 ± 3.01	45.33 ± 2.88**
Relative percentages /%	100.00	98.58	99.09	5.38

Note: The data are presented as means ± SD from six animals per group. Relative percentages were calculated as follows: (experimental group time/normal control group time) × 100. Compared to the saline group, $^{*}P < 0.05$, $^{**}P < 0.01$.

Administration of saline to the buccal mucosa of live toads showed well-defined epithelial structures and orderly arranged cilia. These cilia moved synchronously in the same direction with high frequency and vigor (Fig. 5A). No significant changes in cilia morphology were observed in the normal control group, and ciliary motility persisted for approximately 12 h.

Application of the MAT-OMT in-situ gel and blank in-situ gel matrix resulted in ciliary morphology and motion comparable to the saline group, indicating negligible ciliotoxicity from the in-situ gel and supporting the formulation's suitability for nasal administration (Fig. 5B, and C).

In contrast, treatment with 1% sodium deoxycholate resulted in complete absence of cilia movement and barely discernible intact cilia. The visible detachment of epithelial appendages indicated severe damage to the buccal mucosa and the irreversible inhibition of ciliary movement by sodium deoxycholate (Fig. 5D).

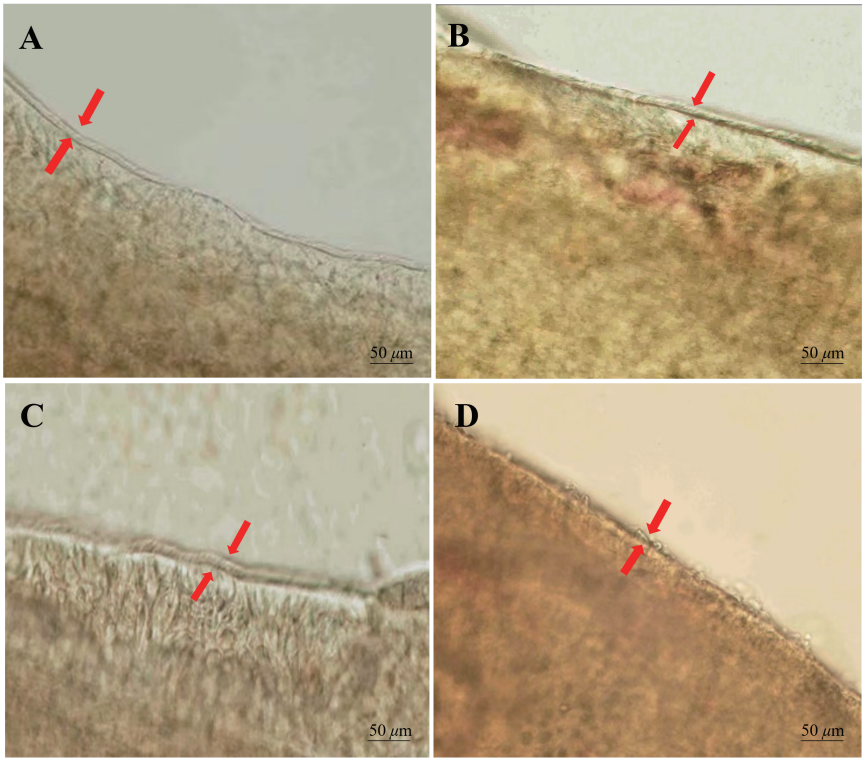

A: saline group; B: MAT-OMT in-situ gel group; C: blank in-situ gel; D: sodium deoxycholate group

Fig. 5 Effect of the MAT-OMT in-situ gel on palatal ciliary morphology

3.5 MAT-OMT in-situ gel treatment alleviates AR symptoms and nasal mucosa injury in a guinea pig AR model

As shown in Fig. 6A, the normal control group had a low pre-treatment behavioral score of 1.17, while all other groups exhibited significantly elevated baseline scores (7.67 ± 0.82, $^{\#\#}P < 0.01$), confirming successful induction of the AR model (threshold > 5 points). Post-treatment evaluation showed marked symptom improvement across all therapeutic groups, with behavioral scores declining below 5 points. The MAT (4.50 ± 1.22), OMT (4.83 ± 1.17), MAT-OMT (4.17 ± 0.75), and budesonide (3.50 ± 0.55) groups all demonstrated statistically significant reductions compared to the AR model group ($^{**}P < 0.01$), confirming therapeutic efficacy against allergic manifestations (nasal itching, sneezing, rhinorrhea). Notably, the MAT-OMT combination showed comparable effectiveness to

budesonide ($P > 0.05$ for intergroup comparison), suggesting an equivalent clinical performance between the experimental formulation and positive control.

As shown in Fig. 6 (B–G), the saline group (Fig. 6B) showed intact cilia without damage to the nasal mucosa, with a well-organized and regular epithelial structure (Fig. 6B-1). The cells appeared uniform with distinct margins and complete morphologies, and were loosely arranged (Fig. 6B-2). In the AR group (Fig. 6C), severe ciliary destruction was observed, with minimal cilia-related structures remaining in the nasal mucosa. The extensive loss of epithelial cells indicated a chaotic and damaged appearance (Fig. 6C-1). The underlying lamina propria exhibited severe edema (Fig. 6C-2), with a loose collagen arrangement and infiltration of numerous lymphocytes and a few neutrophils. In the MAT, OMT, and MAT-OMT groups (Fig. 6D, E, and F), the mucosal epithelial structure remained intact (Fig. 6D-1, E-1, and F-1), with noticeable improvements in edema. Connective tissue displayed a loose arrangement with slight inflammatory cell infiltration (Fig. 6D-2, E-2, and F-2). While mild edema and cell proliferation were still observed in the MAT and OMT groups, the MAT-OMT group showed almost no edema or proliferation, indicating a superior therapeutic effect compared to single-drug treatments. The budesonide group (Fig. 6G) exhibited relatively intact cilia and epithelial cells in the nasal mucosa (Fig. 6G-1), with mild congestion and edema in the lamina propria. A loose arrangement of collagen fibers was accompanied by a minor infiltration of eosinophils and inflammatory cells, demonstrating a certain degree of therapeutic efficacy (Fig. 6G-2).

As shown in Fig. 6 (H–J), the AR model group exhibited significant immunological alterations compared to normal controls: serum IgE levels increased from 21.64 to 57.02 μg/mL ($^{\#\#}P < 0.01$), IL-4 concentrations rose from 3.78 to 12.06 pg/mL ($^{\#\#}P < 0.01$), while IFN-γ levels decreased from 14.34 to 4.56 pg/mL ($^{\#\#}P < 0.01$), collectively confirming successful AR induction. All therapeutic interventions demonstrated marked immunomodulatory effects versus the AR model group, reducing IgE and IL-4 while elevating IFN-γ ($^{**}P < 0.01$ for all parameters). While budesonide showed the most pronounced therapeutic effect, the MAT-OMT combination therapy was superior to monotherapy in IgE suppression ($^{\$\$}P < 0.01$) and showed no significant difference of the therapeutic efficacy from budesonide ($P > 0.05$ for all three biomarkers).

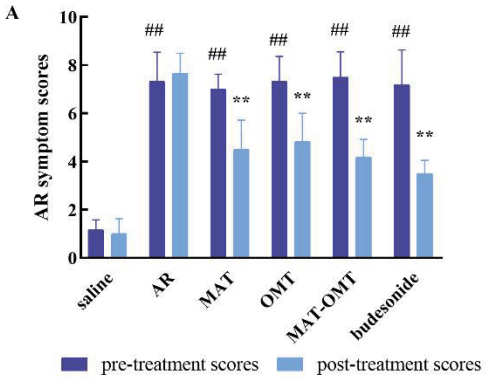

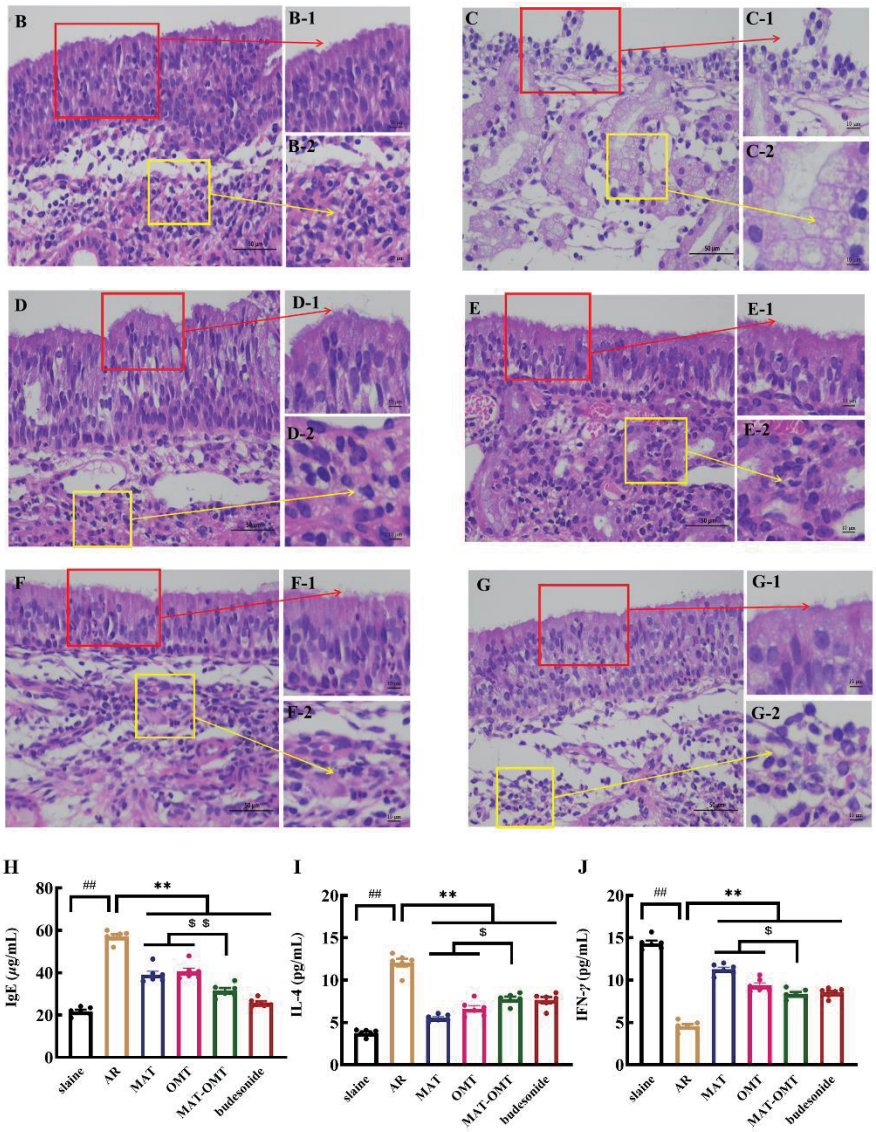

A: AR guinea pig symptom composite score (nasal itching, sneezing, and rhinorrhea). (The data are presented as means ± SD from six animals per group. $^{\#}P < 0.05$; $^{\#\#}P < 0.01$; $^{*}P < 0.05$; $^{**}P < 0.01$; one-way ANOVA).

B–G: Histopathological sections of the nasal mucosa of guinea pigs with AR in each group (B: saline group; C: AR group; D: MAT group; E: OMT group; F: MAT-OMT group; G. budesonide group).

H–J: Inflammatory cytokine concentrations of IgE (H), IL-4 (I), and IFN-γ (J) in the sera of the AR guinea pig model were measured by ELISA. (The data are presented as means ± SD from six independent experiments. Saline group vs. the model group, $^{\#}P < 0.05$, $^{\#\#}P < 0.01$, AR group vs. the model group, $^{*}P < 0.05$, $^{**}P < 0.01$, and the combined group vs. the single drug group, $^{\$}P < 0.05$, $^{\$\$}P < 0.01$; one-way ANOVA.

Fig. 6 MAT-OMT in-situ gel treatment alleviates AR symptoms and nasal mucosa injury

Notably, the model group exhibited a typical Th2-dominant pathological characteristics, as evidenced by significantly elevated IgE and IL-4 levels ($^{**}P < 0.01$). All treatment groups showed markedly reduced IgE and IL-4 levels ($^{**}P < 0.01$). Concurrently, IFN-γ levels were significantly elevated ($^{**}P < 0.01$). These findings demonstrate that immune response was modulated in AR through elevating anti-inflammatory factors and reducing pro-inflammatory cytokines, thereby restoring

the Th1/Th2 balance and further supporting their therapeutic potential. Importantly, the MAT-OMT in-situ gel outperformed monotherapy in terms of therapeutic efficacy.

4 Discussion

This study developed a thermosensitive in-situ gel containing MAT-OMT using a ternary Pluronic F127/F68/glycerol matrix. The gelation temperature was optimized to 33.2 °C via Box-Behnken design. The optimized formulation exhibited rapid sol-gel transition at nasal temperature (33.5 °C), facilitating precise localization and prolonged retention following intranasal administration.

Regarding the release mechanism, although MAT and OMT differ significantly in water solubility, both compounds demonstrated highly consistent release profiles from the Pluronic in-situ gel. This consistent release behavior stems from the molecular-level dissolution of both drugs in the gel precursor solution (sol state) at the administered dosage. Such a state of molecular dissolution results in a homogeneous dispersed system, thereby minimizing the impact of their inherent solubility differences on the release kinetics. Consequently, upon gelation, their release is predominantly controlled by the structure of the gel network, significantly reducing the influence of their solubility differences. Release kinetic modeling revealed that the release behaviors of MAT and OMT followed those of Ritger-Peppas and Weibull models. Analysis using the Ritger-Peppas model indicated that the *n*-values of the diffusion exponent (MAT: 0.5086; OMT: 0.5920) fell within the range for anomalous transport ($0.5 < n < 1$), approaching the diffusion-dominated boundary ($n = 0.5$). This suggests a release mechanism primarily driven by drug diffusion, moderated by synergistic erosion of the polymer matrix. The Weibull model parameter β (MAT: 0.4161; OMT: 0.3087) further supports this mechanism, with $\beta < 1.0$ indicating initial rapid release followed by gradual attenuation—consistent with diffusion-erosion synergy. In summary, the release of MAT and OMT from the Pluronic gel follows an anomalous transport mechanism dominated by diffusion and assisted by erosion [39]. This synchronized *in vitro* release behavior provides a drug release kinetic foundation for co-delivery of both drugs to AR lesion sites and is expected to enhance their synergistic therapeutic effect.

The MAT-OMT in-situ gel showed negligible ciliotoxicity, confirming its nasal biocompatibility. In AR guinea pig models, the synergistic therapeutic effect of OMT and MAT surpassed that of monotherapy. This synergistic effect are attributed to sustained efficacy with reduced toxicity and broadened pharmacological targets. From a molecular structural perspective, OMT exhibits enhanced hydrophilicity compared with MAT because of the introduction of an oxygen atom at the nitrogen-1 position, resulting in reduced transmembrane capacity [40]. In contrast, MAT demonstrates strong transmembrane permeability and rapid metabolism, leading to short therapeutic efficacy. Although OMT has weaker transmembrane permeability, it can be metabolized into active MAT, acting as both a prodrug and a reservoir for MAT, thereby prolonging drug efficacy [9,13]. Notably, high concentrations of MAT are toxic [10]. This discrepancy may arise because the combined use of OMT and MAT prevents toxicity by avoiding excessive local drug concentrations of MAT in the nasal mucosa, while leveraging the metabolic conversion properties of OMT to extend local drug retention. This approach achieves a dynamic balance between transmembrane efficiency and sustained pharmacological action. In terms of improvement of inflammatory cytokine modulation, although the OMT-MAT combination did not significantly outperform monotherapies in reducing serum IL-4 or elevating IFN-γ levels, it demonstrated improved

efficacy in alleviating behavioral symptoms, promoting histopathological recovery (as evidenced by H&E staining), and reducing serum IgE levels. These findings collectively indicate a distinct pharmacodynamic advantage of the combination strategy. In addition, although MAT and OMT share overlapping molecular targets [41], OMT uniquely suppresses SADBE-induced allergic inflammation by modulating cytokine expression and inhibiting TRPA1/TRPV1 mRNA expression [42].

Although the MAT-OMT in-situ gel demonstrates promising preclinical efficacy and safety in guinea pig AR models, clinical translation requires further validation in higher mammalian species. To bridge this gap, future work will include evaluation of the formulation stability under long-term and accelerated conditions, trials in non-human primates, and elucidation of the synergy between MAT and OMT. Spatial transcriptomics or single-cell sequencing will be employed to dynamically track their differential regulatory effects on immune microenvironment cell subsets (e.g., Th2 cells, mast cells, and epithelial barrier cells) in the nasal mucosa, thereby uncovering the cellular and molecular logic underlying immune balance restoration. These investigations are postulated to provide theoretical support for the development of modernized nasal drug delivery systems from traditional Chinese medicine that prioritize both efficacy and safety.

5 Conclusion

In this study, traditional Chinese medicine was successfully integrated with modern formulation technology to develop a MAT-OMT-loaded nasal in-situ gel. In a guinea pig AR model, the gel demonstrated significant therapeutic efficacy: it corrected Th1/Th2 immune imbalance, improved the histopathological features of nasal tissues, and reduced inflammatory cytokine levels. In addition, its therapeutic effect was comparable to that of budesonide, a clinically used positive control drug, while exhibiting no ciliotoxicity and excellent safety. This study not only validates the scientific value of traditional Chinese medicine in treating AR, but also overcomes the limitations of traditional applications through the design of a novel drug delivery system. Our findings provide innovative insights into the development of natural product-based nasal therapeutics.

Funding sources

This research was supported by the National Key Research and Development Program of China (No. 2024YFE0111300).

Data availability

The datasets used and/or analysed during the current study are available from the corresponding author on reasonable request.

Disclosure

The authors declare that they have no known competing financial interests or personal relationships that could have appeared to influence the work reported in this paper.

References

[1] Li P, Tsang MSM, Kan LLY, et al. The Immuno-Modulatory Activities of Pentaherbs Formula on Ovalbumin-Induced Allergic Rhinitis Mice via the Activation of Th1 and Treg Cells and Inhibition of Th2 and Th17 Cells. Molecules, 2022, 27: 239.

[2] Rosenfield L, Keith PK, Quirt J, et al. Allergic rhinitis. Allergy Asthma Clin Immunol, 2024, 20: 74.

[3] Zhang Z, Kang H. Protective effect of Asarum sieboldii essential oil on ovalbumin induced allergic rhinitis in

rat. Biosci Rep, 2020, 40: 1-8.

[4] Dykewicz MS, Wallace DV, Amrol DJ, et al. Rhinitis 2020: A practice parameter update. J Allergy Clin Immun, 2020, 146: 721-767.

[5] Chen Y, Wang J, Wu L, et al. Efficacy of Chinese herbal medicine on nasal itching in children with allergic rhinitis: a systematic review and meta-analysis. Front Pharmacol, 2023, 14: 1240917.

[6] Zhang Z, Zhang K, Qin Z, et al. Observation of the efficacy of traditional Chinese medicine Sophora radix on allergic rhinitis. J Beijing Med Univ, 1990, 03: 233.

[7] Chen X, Liu P, Mao Y, et al. Research Advancements in Pharmacological Activities and Mechanisms of Matrine. Pharmacogn Mag, 2024, 20: 189-205.

[8] Wang R, Wang Y, Yang Q, et al. Xiaoqinglong decoction improves allergic rhinitis by inhibiting NLRP3-mediated pyroptosis in BALB/C mice. J Ethnopharmacol, 2024, 321: 117490.

[9] Tang L, Dong LN, Peng XJ, et al. Pharmacokinetic characterization of oxymatrine and matrine in rats after oral administration of radix Sophorae tonkinensis extract and oxymatrine by sensitive and robust UPLC-MS/MS method. J Pharm Biomed Anal, 2013, 83: 179-185.

[10] Feng W, Kao TC, Jiang J, et al. The dynamic equilibrium between the protective and toxic effects of matrine in the development of liver injury: a systematic review and meta-analysis. Front Pharmacol, 2024, 15: 1315584.

[11] Lu S, Xiao X, Cheng M. Matrine inhibits IL-1β-induced expression of matrix metalloproteinases by suppressing the activation of MAPK and NF-κB in human chondrocytes in vitro. Int J Clin Exp Patho, 2015, 8: 4764-4772.

[12] Zhang Z, Pan J, Zhu T, et al. Oxymatrine screened from Sophora flavescens by cell membrane immobilized chromatography relieves histamine-independent itch. J Pharm Pharmacol, 2021, 73: 1617-1629.

[13] Fan R, Liu R, Ma R, et al. Determination of oxymatrine and its activemetabolitematrine in human plasma after administration of oxymatrine oral solution by high-performance liquid chromatography coupled with mass spectrometry. Fitoterapia, 2013, 89: 271-277.

[14] Wolburg H, Wolburg-Buchholz K, Sam H, et al. Epithelial and endothelial barriers in the olfactory region of the nasal cavity of the rat. Histochem Cell Biol, 2008, 130: 127-140.

[15] Karavasili C, Fatouros DG. Smart materials: In situ gel-forming systems for nasal delivery. Drug Discov Today, 2016, 21: 157-166.

[16] Wang W, Wat E, Hui PCL, et al. Dual-functional transdermal drug delivery system with controllable drug loading based on thermosensitive poloxamer hydrogel for atopic dermatitis treatment. Sci Rep, 2016, 6: 24112.

[17] Corazza E, di Cagno MP, Bauer-Brandl A, et al. Drug delivery to the brain: In situ gelling formulation enhances carbamazepine diffusion through nasal mucosa models with mucin. Eur J Pharm Sci, 2022, 179: 106294.

[18] Alparslan AL, Yildiz Türkyilmaz G, Kozaci LD, et al. Thermoreversible Gel Formulation for the Intranasal Delivery of Salmon Calcitonin and Comparison Studies of In Vivo Bioavailability. Turk J Pharm Sci, 2023, 20: 127-140.

[19] Agrawal M, Saraf S, Saraf S, et al. Stimuli-responsive In situ gelling system for nose-to-brain drug delivery. J Control Release, 2020, 327: 235-265.

[20] Kolawole OM, Cook MT. In situ gelling drug delivery systems for topical drug delivery. Eur J Pharm Biopharm, 2023, 184: 36-49.

[21] Shriky B, Kelly A, Isreb M, et al. Pluronic F127 thermosensitive injectable smart hydrogels for controlled drug delivery system development. J Colloid Interface Sci, 2020, 565: 119-130.

[22] Al Khateb K, Ozhmukhametova EK, Mussin MN, et al. In situ gelling systems based on Pluronic F127/Pluronic F68 formulations for ocular drug delivery. Int J Pharm, 2016, 502: 70-79.

[23] du Sert NP, Hurst V, Ahluwalia A, et al. The arrive guidelines 2.0: Updated guidelines for reporting animal research. PLoS Biol, 2020, 18: e3000410.

[24] Schmolka IR. Artificial skin. I. Preparation and properties of pluronic F-127 gels for treatment of burns. J Biomed Mater Res, 1972, 6: 571-582.

[25] Barakat SS, Nasr M, Ahmed RF, et al. Intranasally administered in situ gelling nanocomposite system of dimenhydrinate: Preparation, characterization and pharmacodynamic applicability in chemotherapy induced emesis model. Sci Rep, 2017, 7: 9910.

[26] Cunha S, Swedrowska M, Bellahnid Y, et al. Thermosensitive in situ hydrogels of rivastigmine-loaded lipid-based nanosystems for nose-to-brain delivery: characterisation, biocompatibility, and drug deposition studies. Int J Pharm, 2022, 620: 121720.

[27] Schilling AL, Kulahci Y, Moore J, et al. A thermoresponsive hydrogel system for long-acting corticosteroid delivery into the paranasal sinuses. J Control Release, 2021, 330: 889-897.

[28] Eleraky NE, El-Badry M, Omar MM, et al. Curcumin Transferosome-Loaded Thermosensitive Intranasal in situ Gel as Prospective Antiviral Therapy for SARS-Cov-2. Int J Nanomedicine, 2023, 18: 5831-5869.

[29] Verekar RR, Gurav SS, Bolmal U. Thermosensitive mucoadhesive in situ gel for intranasal delivery of Almotriptan malate: Formulation, characterization, and evaluation. J Drug Deliv Sci Technol, 2020, 58: 101778.

[30] Ravi PR, Aditya N, Patil S, et al. Nasal in-situ gels for delivery of rasagiline mesylate: Improvement in bioavailability and brain localization. Drug Deliv, 2015, 22: 903-910.

[31] Qian S, Wong YC, Zuo Z. Development, characterization and application of in situ gel systems for intranasal delivery of tacrine. Int J Pharm, 2014, 468: 272-282.

[32] Pang L, Zhu S, Ma J, et al. Intranasal temperature-sensitive hydrogels of cannabidiol inclusion complex for the treatment of post-traumatic stress disorder. Acta Pharm Sin B, 2021, 11: 2031-2047.

[33] Chu K, Chen L, Xu W, et al. Preparation of a paeonol-containing temperature-sensitive in situ gel and its preliminary efficacy on allergic rhinitis. Int J Mol Sci, 2013, 14: 6499-6515.

[34] Miao M, Xiang L, Miao Y. Specification for preparation of allergic rhinitis animal model (draft). Chin Tradit Herb Drugs, 2018, 49: 50-57.

[35] Jing Z, Li W, Liao W, et al. Fructus Xanthii and Magnolia liliiflora Volatile Oils Liposomes-Loaded Thermosensitive in situ Gel for Allergic Rhinitis Management. Int J Nanomedicine, 2024, 19: 1557-1570.

[36] Bao Y, Wu Z, Zhu X, et al. The study of the role of purified anti-mouse CD193 (CCR3) antibody in allergic rhinitis mouse animal models. Sci Rep, 2024, 14: 1059.

[37] Nasr M. Development of an optimized hyaluronic acid-based lipidic nanoemulsion co-encapsulating two polyphenols for nose to brain delivery. Drug Deliv, 2016, 23: 1444-1452.

[38] Ide T, Izawa K, Diono W, et al. Intranasal administration of ceramide liposome suppresses allergic rhinitis by targeting CD300f in murine models. Sci Rep, 2024, 14: 8398.

[39] Gomes-Filho MS, Oliveira FA, Barbosa MAA. Modeling the diffusion-erosion crossover dynamics in drug release. Phys Rev E, 2022, 105: 044110.

[40] Yang F, Zhong W, Cao J, et al. Matrine induces V-ATPase-dependent cytoplasmic vacuolation and inhibits the function of the lysosome in leukemia cells. PHSA, 2024, 2: 100013.

[41] Lu M, Zhang Q, Chen K, et al. The regulatory effect of oxymatrine on the TLR4/MyD88/NF-κB signaling pathway in lipopolysaccharide-induced MS1 cells. Phytomedicine, 2017, 36: 153-159.

[42] Zhu T, Zhou D, Zhang Z, et al. Analgesic and antipruritic effects of oxymatrine sustained-release microgel cream in a mouse model of inflammatory itch and pain. Eur J Pharm Sci, 2020, 141: 105110.